Renewable Energy 94 (2016) 55–71

Contents lists available at ScienceDirect

Renewable Energy

journal homepage: www.elsevier.com/locate/renene

Climatic parameters for building energy applications: A temporal-geospatial assessment of temperature indicators

Monjur Mourshed

BRE Centre for Sustainable Engineering, School of Engineering, Cardiff University, Cardiff, CF24 3AA, United Kingdom

ARTICLE INFO

Article history:
Received 27 October 2015
Received in revised form
2 March 2016
Accepted 3 March 2016

Keywords:
Climate
Temperature
Degree-days
ASHRAE-HOF
Geospatial distribution
Energy applications

ABSTRACT

Understanding the climate and location aspects are usually the first step in energy applications – from buildings to renewable energy. With so many of the renewable energy sources being significantly dependent on weather, it is essential that the temporal and geospatial variability and distribution of climatic design parameters are investigated for effective planning and operation. ASHRAE-HOF is the most widely used climatic design conditions database for building energy and HVAC professionals, but gaps exist in the literature on the geospatial and temporal distributions of the HOF dataset. This research explored geospatial distributions of key HOF (2009) climatic parameters: temperature (dry-bulb, wet-bulb, dew-point and mean) and degree-days at various temporal scales. Identified spatial variability illustrate the effects of latitude, elevation, landuse and nearest coastline. Observed trends agree with conventional wisdom; however, sparse coverage in populated areas such as Africa and Asia diminish the versatility of the database. Variations in temperature exist, even between closely spaced sites – emphasizing the need to use location-specific data for enhancing the accuracy of the weather-related analysis. Moreover, latitudinal similarities in the distribution offer potential in identifying candidate locations for reciprocal transfer of knowledge on environmental design and operation.

1. Introduction

The need to reduce lifecycle carbon emissions from buildings to mitigate the impacts of climate change mandates that the efficiency of a building and its systems are optimized right from the beginning – at the earliest in the design process. Most of the decisions affecting a building's energy and environmental performance are taken during this stage. Mistakes and *less than optimum* design decisions are often carried forward in subsequent stages as early-stage decisions are difficult to alter. Complexities arise mainly due to the fragmented nature of the industry [1] and the involvement of many disciplines with varying understanding of the problem and work practices [2,3]. As one of the major boundary conditions of building design, the climate of a site plays a vital role in identifying and formulating design strategies [4]. An understanding of site climate and resulting climatic design conditions is, therefore, essential for effective design and operation of energy efficient buildings. Climatic design conditions, a summary of climate attributes and derived indicators, are routinely used to formulate and verify strategies for the design of building layout, form and fenestration – as well as for the design and operation of heating, refrigeration, ventilation and air-conditioning systems [5].

The analysis of precedents is an integral part of learning and practice of design [6–8]. Precedents are often exemplars that act as a benchmark and are used by designers (student/apprentice and practitioners) to glean concepts or ideas relevant to the problem they are trying to solve. Designers also learn from failures of their work or that of their peers. In this sense, precedents can also be negative ones, illustrating some failure [6]. In addition to having an understanding of the climate of the design site, it is also essential that the climatic features of the precedent site are understood, and its differences with the design site's climate are reconciled while gleaning relevant knowledge. Geospatial distributions of climatic parameters are useful in these circumstances where knowledge is often extracted from contextual observations of the effectiveness of a particular feature/strategy. Moreover, contextual observations are often carried out in situations where detailed information about buildings is not always available. Inference from observation and experience is, therefore, widely used and is more often than not the most effective strategy. The lack of knowledge of the distribution of

E-mail address: MourshedM@Cardiff.ac.uk.
URL: http://monjur.mourshed.org/

http://dx.doi.org/10.1016/j.renene.2016.03.021

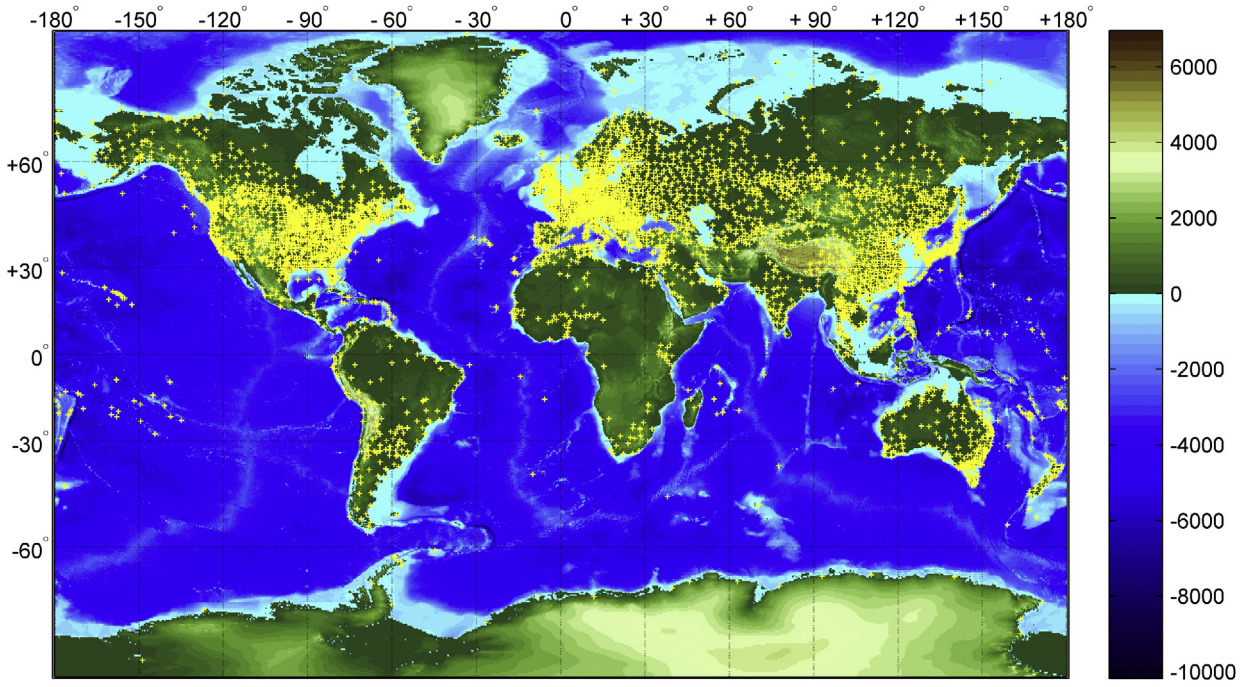

Fig. 1. Locations of 5511 meteorological stations included in this study. The colormap represents altitude (m).

climate parameters may make it difficult, even impossible, to extract useful knowledge, if precedent and design sites are located in distinct climatic regions.

Projected changes in climate, in particular, global increases in temperature, are likely to alter the present-day climate characteristics of most locations. The magnitudes of the projected changes are uneven; i.e., not all places on earth will experience warming at the same rate [9]. An understanding of the distribution of changing parameters will help in identifying vulnerable regions and develop appropriate technologies and policies. While contemporary building regulations and policies are predominantly aimed at energy conservation and carbon emissions reduction, there is evidence of a gradual move towards adaptation to the inevitable changes in climate [10,11]. It is the identification of adaptation strategies where the investigations on distribution can offer significant leverage. The understanding of the behavior of buildings and occupants in future climates of a site can be thought of as an example. As the future climate is only a projection based on scenarios, it is difficult to ascertain how people will behave or adapt to the changes, as it does not exist yet. One can, however, get an idea of the physical and psychophysiological effect by studying a present-day climate of another location that is similar in characteristics to the projected future climate of a site. In climatological terms, this is known as an *analog* scenario/climate [12], which can be identified from distribution maps.

Climatic design information from professional bodies and governments are routinely used for the design and operational management of buildings that are responsible for 40% of global energy consumption and resulting greenhouse gas emissions [13]. Despite their routine use, design conditions database lag behind the state-of-the-art developments in climate and meteorology, both in terms of coverage and scope. The use of low resolution data averaged over a large geographic area is commonplace. For example, the underlying method of complying with the overarching European legislation, Energy Performance of Buildings Directive [14] on building energy efficiency relies on single degree-day quantity for large regions, ignoring the geospatial effects of temperature distribution. Such generalizations often result in significant discrepancies between the predicted (during design) and actual (operational) energy use. While, hypothetically, one can make use of detailed and robust climatic data from recognized sources such as IRENA Global Atlas for renewable energy [15], Meteonorm[1] [16] and CRU climate data,[2] in practice, however, there is a lack of evidence on the use of these data by the wider built environment community.

Existing research lacks an understanding of the distribution of climatic design parameters used by the built environment professionals. One of the reasons for this gap is that a *fine* resolution climate dataset covering the earth was not readily available until recently. Other reasons are related to the challenges associated with quality assurance of data and large-scale geospatial analysis. The recent release of a comprehensive climatic design information dataset by the American Society of Heating, Refrigerating and Air-Conditioning (ASHRAE) [5] enables us to construct geospatial distribution maps of climatic parameters and derived indicators, of interest to the built environment community. This paper investigates the geospatial distribution of key climatic design information: temperature and derived parameters at two temporal scales: annual and monthly. The rest of the paper is organized as follows. The source of data and methods for scattered data interpolation and the construction of distribution maps are discussed next, followed by a section on results and contextual discussions. The article ends with concluding remarks.

2. Methods

2.1. Data source

Several sources of data on climate parameters exist with varying

[1] Most of the data in meteonorm are taken from the Global Energy Balance Archive (GEBA), World Meteorological Organization (WMO); however, non-station data are mostly synthetic.

[2] Climatic Research Unit, University of East Anglia. http://cru.uea.ac.uk/data.

temporal and spatial resolution. Based on content and utility, these datasets can be categorized into two: observed weather conditions and processed climatic conditions and climate normals. Observed weather data are historical and contain observations of key weather parameters for some years. An example of such dataset is the UK Met Office MIDAS Land Surface Stations data [17], which contains meteorological values observed at 3-hourly[3] intervals, covering most parts of the globe from 1974 to date. Other notable datasets for renewable energy applications are: International Renewable Energy Agency (IRENA) Global Atlas [15] and Meteonorm [16]. In processed climatic design conditions datasets, raw weather observations from a representative period (typically 30 years, sometimes a decade) of a location are processed using statistical methods to form a typical weather dataset; e.g., typical meteorological year (TMY) [18]. Typical weather data can then be used for the design of buildings and systems. Such processed data are available from professional and national bodies such as ASHRAE [19] and Chartered Institution of Building Services Engineers (CIBSE) [20], as well as from international organizations [21]. Representative climatic design conditions in the form of typical weather data are of interest in this research as the objective is to investigate the global distribution of typical climatic conditions rather than the observations in a particular year.

Climatic design information from *ASHRAE Handbook – Fundamentals* [5] is used in this study. The dataset, often referred to as the *HOF'09* dataset, reportedly contains climatic design conditions for 5564 meteorological stations worldwide, created from an hourly dataset, details of which can be found in Refs. [22,23]. It has been reported that some of the stations such as the Canadian stations from Nova Scotia, Northwest Territories, etc. are reported twice in the HOF'09 dataset [24]. Duplicate stations are, therefore, included only once in this study – reducing the total number of unique stations to 5511. The locations of reporting stations are presented as points on a hybrid bathymetric and topographic map of the world in Fig. 1. The list contains land-based as well as marine stations. The inclusion of data from marine environmental buoys enables the construction of global distribution maps without significant discontinuities. Design conditions in the HOF'09 dataset are constructed from long-term hourly observations of the listed meteorological stations. There are 1085 stations from the United States, 427 from Canada[4] and 3999 from the rest of world. The concentration of stations is higher in some regions; e.g., North America, western Europe, etc. However, the remaining stations are widely distributed and suitable for investigating the distribution of climatic design parameters.

2.2. Investigated climatic parameters

Climatic design information in the HOF'09 dataset includes values of dry-bulb, wet-bulb and dew-point temperature, as well as wind speed with direction at various frequencies of occurrence. Also, annual and monthly heating and cooling degree-days to various base temperatures, as well as parameters to calculate clear-sky irradiance are provided. The climate normals are created using time-series weather observations comprising hourly data. The methodology adopted for creating the dataset has been discussed in detail by Thevenard [23,22]. Data for each location contains hundreds of parameters. Considering their importance in environmental design and operation of buildings, only the following subset has been selected from the HOF'09 dataset for investigation in this research:

- Annual mean temperature, $\overline{T}$ (°C)
- Monthly mean temperature, $\overline{T}_m$ (°C)
- 99.6% Heating dry-bulb temperature, $HDB_{99.6}$ (°C)
- 99.6% Dew-point temperature, $DP_{99.6}$ (°C)
- 0.4% Cooling dry-bulb temperature, $CDB_{0.4}$ (°C)
- 0.4% Mean coincident wet-bulb temperature, $MCWB_{0.4}$ (°C)
- Heating degree-days at 18.3 °C (65 °F) base temperature, $HDD_{18.3}$ (°C-day)
- Cooling degree-days at 18.3 °C (65 °F) base temperature, $CDD_{18.3}$ (°C-day)

Mean temperatures, $\overline{T}$ and $\overline{T}_m$, are the means of temperature over their respective periods of observation. Heating dry-bulb temperature, $HDB_{99.6}$ and dew-point temperature, $DP_{99.6}$ are 99.6 percentile values in the typical year. Similarly, cooling dry-bulb temperature, $CDB_{0.4}$ and mean coincident wet-bulb temperature, $MCWB_{0.4}$ are 0.4 percentile values in the typical year. 99.6% design conditions are used for sizing heating equipment. Dew-point temperature is intended for use in humidification applications. 0.4% design conditions are often used for sizing cooling equipment such as chillers or air-conditioning units. Heating and cooling degree-days are used for estimating energy consumption over a reporting period – typically annual, sometimes monthly [25–27], and the assessment of the impact of climate change on heating and cooling energy demand from buildings [28]. They are also used for

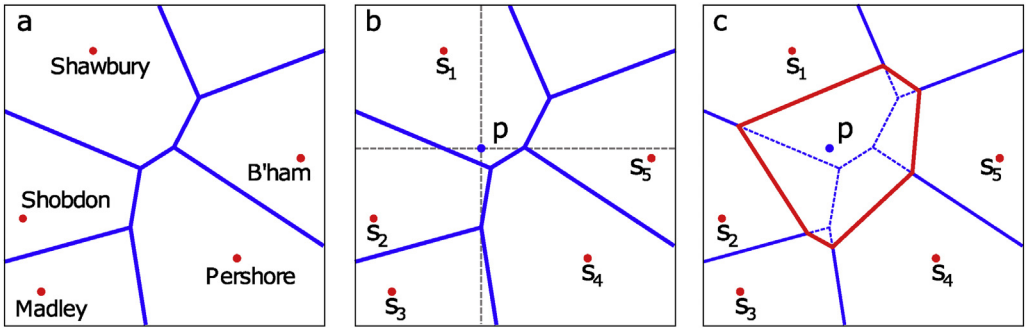

Fig. 2. Natural neighbor interpolation using Voronoi tessellation. (a) Voronoi diagram of five stations, (b) Voronoi sites and target point, *p* and (c) Changes in the Voronoi diagram due to *p*.

[3] Data for United Kingdom in MIDAS are available at a higher resolution (hourly and sub-hourly) for various weather parameters since 1853.

[4] Note that the number of Canadian stations in the HOF'09 dataset is 480, of which 53 are duplicates. The number of unique stations is, therefore, 427 = 480 – 53.

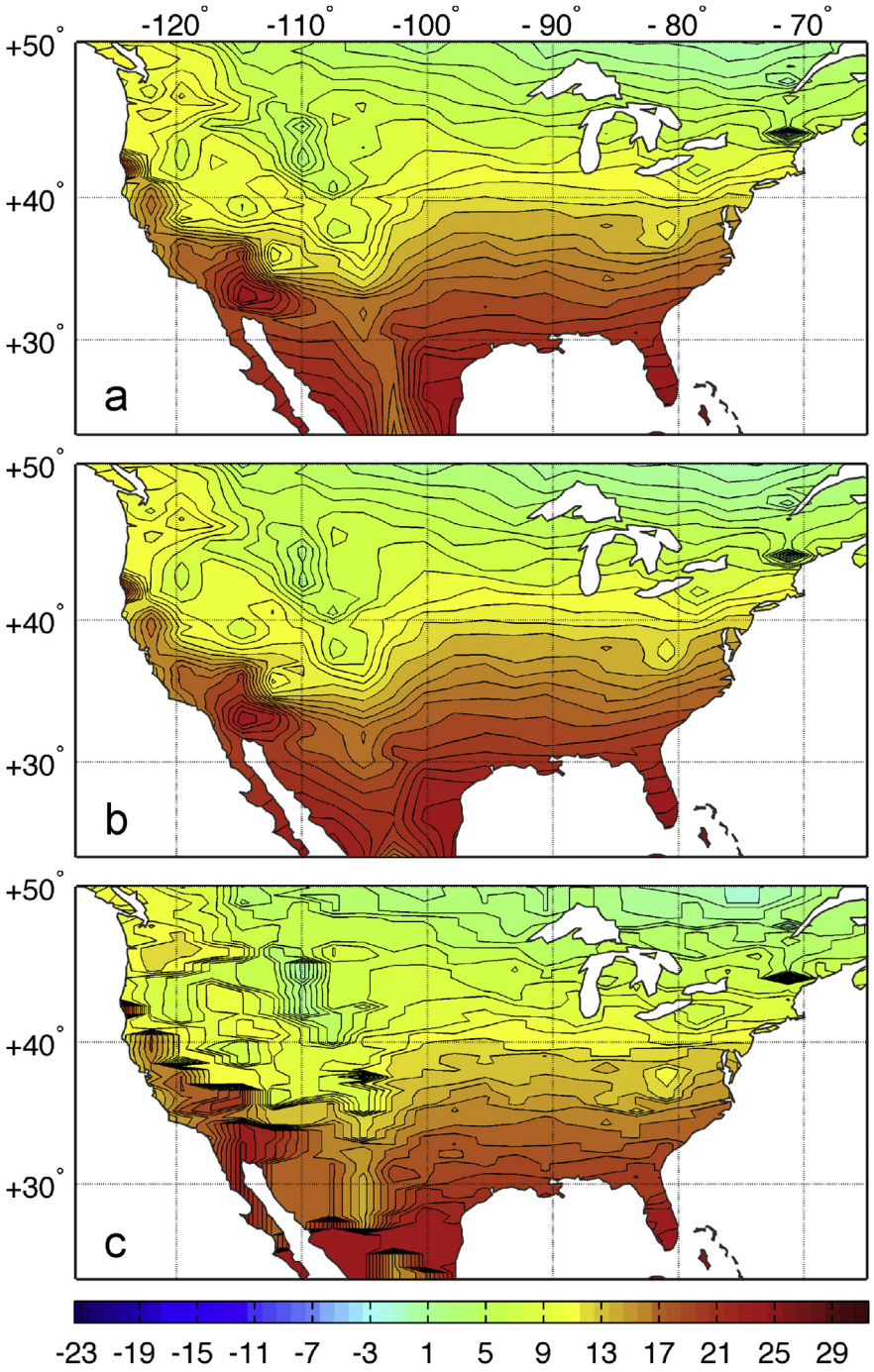

Fig. 3. The effect of interpolation method on the contouring of annual mean temperature, $\overline{T}$ (° C): (a) triangulation with linear interpolation, (b) natural neighbor and (c) nearest neighbor.

standards-based compliance as stipulated in the ASHRAE standard 90.1–2010 [29]. Note that, a different base temperature (10 °C or 50° F) is often used for ASHRAE 90.1 compliant calculations. In this paper, $CDD_{18.3}$; i.e., cooling degree-days at 18.3 °C base is investigated to maintain consistency while comparing the patterns of heating and cooling degree-days.

Degree-day records in the HOF′09 dataset were created using Schoenau and Kehrig's method [30]. Heating degree-days, HDD_b to base T_b were calculated from:

$$HDD_b = Ns_d[Z_bF(Z_b) + f(Z_b)] \quad (1)$$

where N is the number of days in the month, Z_b is the difference between base temperature, T_b and monthly mean temperature, $\overline{T}_m$, normalized by the standard deviation (SD) of the daily mean temperature, s_d, which can be found from the following expression:

$$Z_b = \frac{T_b - \overline{T}_m}{s_d} \quad (2)$$

Function f is the Gaussian probability density function with

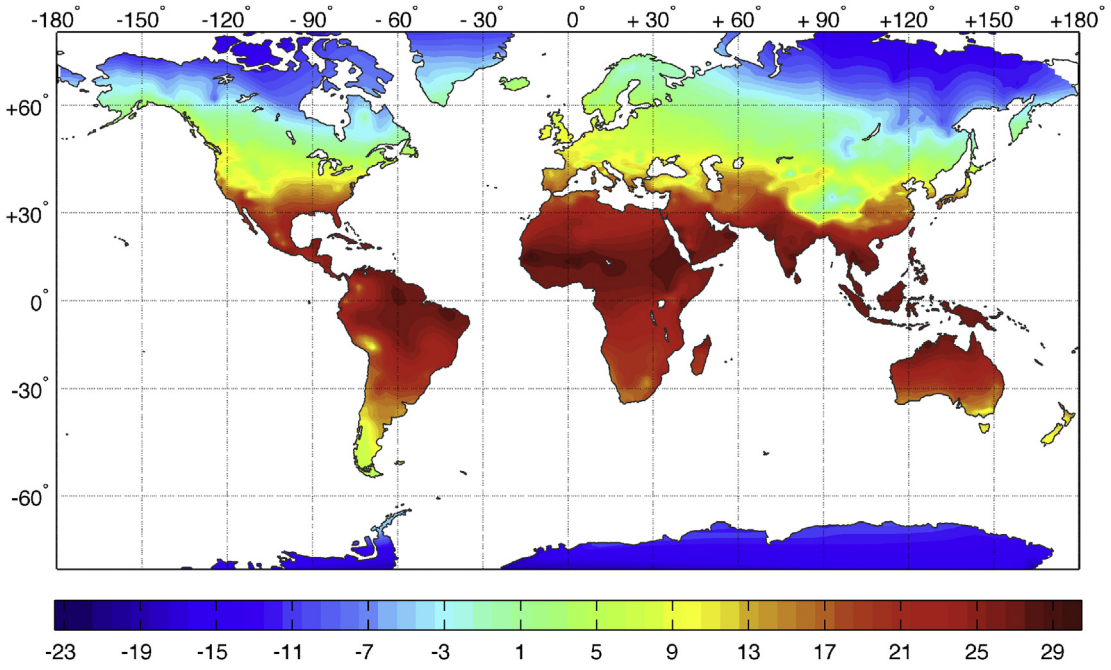

Fig. 4. Global distribution of annual mean temperature, $\overline{T}$ (° C).

mean 0 and SD 1, and function F is the equivalent cumulative normal probability function:

$$f(Z) = \frac{1}{2\pi}\exp\left(\frac{-Z^2}{2}\right) \tag{3}$$

$$F(Z) = \int_{-\infty}^{z} f(z)dz \tag{4}$$

Cooling degree-days were calculated using the Equation (5), which is similar to the method for calculating heating degree-days, described in Equation (1).

$$CDD_b = Ns_d[Z_b F(Z_b) + f(Z_b)] \tag{5}$$

However, Z_b for cooling degree-days has the following from:

$$Z_b = \frac{\overline{T}_m - T_b}{s_d} \tag{6}$$

2.2.1. Mapping

Two dimensional contour maps are created to investigate the geospatial distribution of climatic design parameters. The latitudinal extent of the map is between 75° N and 75° S. The longitudinal extent is between and 180 °E and 180 °W. Irregularly located scattered design conditions data are interpolated to the nodes of a 0.5° of latitude by 0.5° of longitude lattice; i.e., the extent of the map is divided into 150 × 360 equally spaced grids. For interpolating the scattered geo-referenced data into this synthetic lattice, three interpolation techniques are investigated for their suitability and discussed next. Following the tests on suitability, *Natural neighbor interpolation*, developed by Sibson [31], is selected as the method for implementation in this research. Interpolated data are used to produce a continuous 3D surface, which is then transformed into contours with different level steps for different parameters. The resulting contours are plotted as a map, based on Miller projection. The area between contoured isolines are filled with a solid color, representing the z-value in the colormap. Oceans are masked as sea-surfaces are not an area of interest for building applications. Masked oceans also make it easy to identify the shape and features of land masses.

2.3. Spatial interpolation methods

Interpolation typically involves the generation of an evenly spaced rectangular grid or lattice covering the study region and then the estimation of the surface value or height for every grid intersection or cell. In deterministic interpolation methods, a simple linear expression, of the following form is used to compute the grid values [32]:

$$z_k = \sum_{i=1}^{n} \lambda_i z_i \tag{7}$$

where z_k is the z-value to be estimated for location k and λ_i is the estimated weight applied to the known value z_i at point (x_i,y_i). z_k is a simple weighted average; therefore, the sum of the weights, λ_i needs to be one, shown in Equation (8).

$$\sum_{i=1}^{n} \lambda_i = 1 \tag{8}$$

The task is to determine the optimum weights to be used in Equation (7). For spatially distributed data, measured points closer to z_k are more likely to be similar to z_k than those further away. Several variants of interpolation techniques exist and they differ in the way the subset of points (i.e., points closer to z_k) is defined and the weights, λ_i are estimated. A number of techniques have previously been applied for the interpolation of climatic normals, an investigation into the suitability of them in different geographies can be found in Ref. [33]. Among the commonly used interpolation techniques, *triangulation with linear interpolation*, *nearest neighbor*

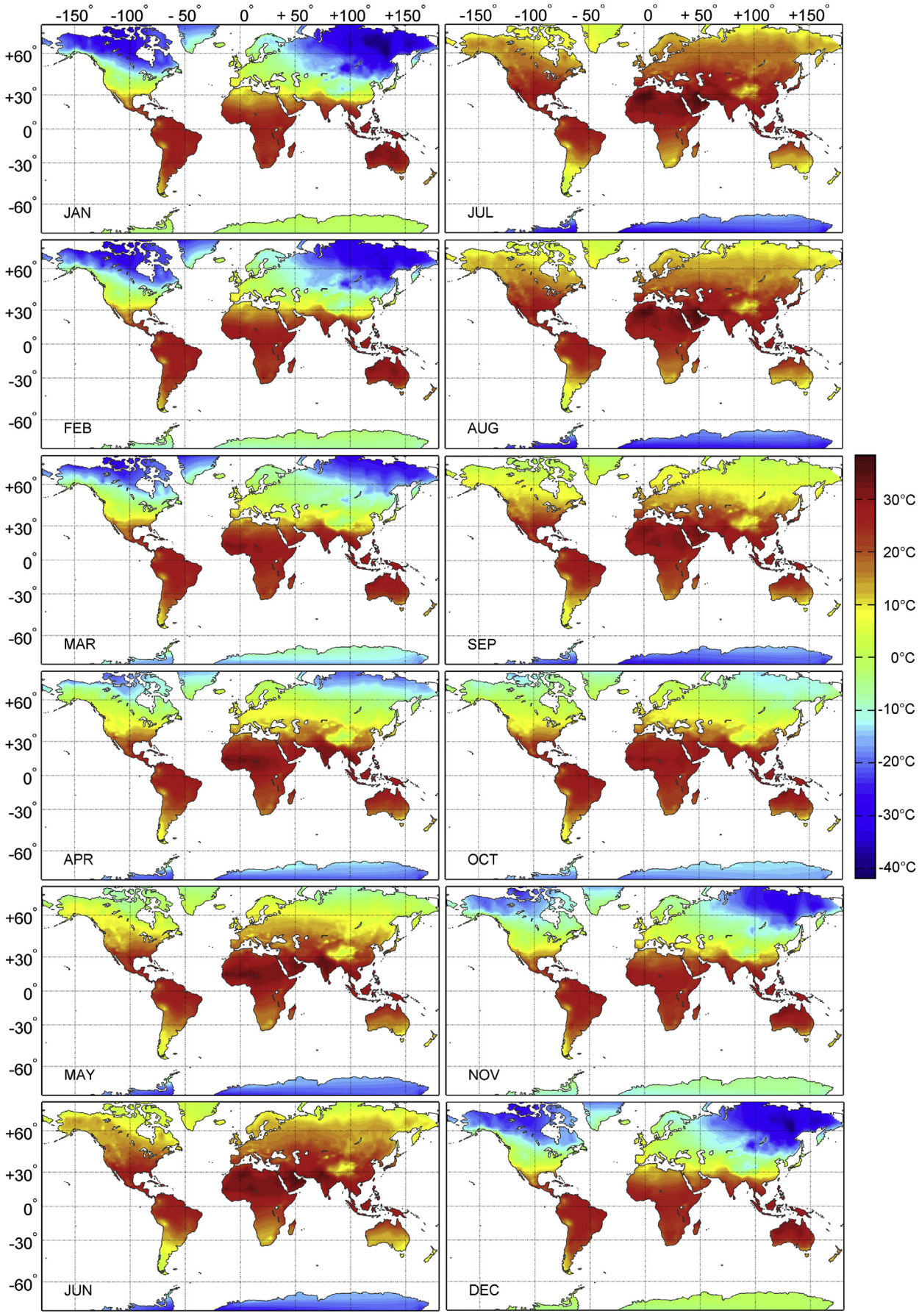

Fig. 5. Temporal distribution of mean temperature, $\overline{T}_m$.

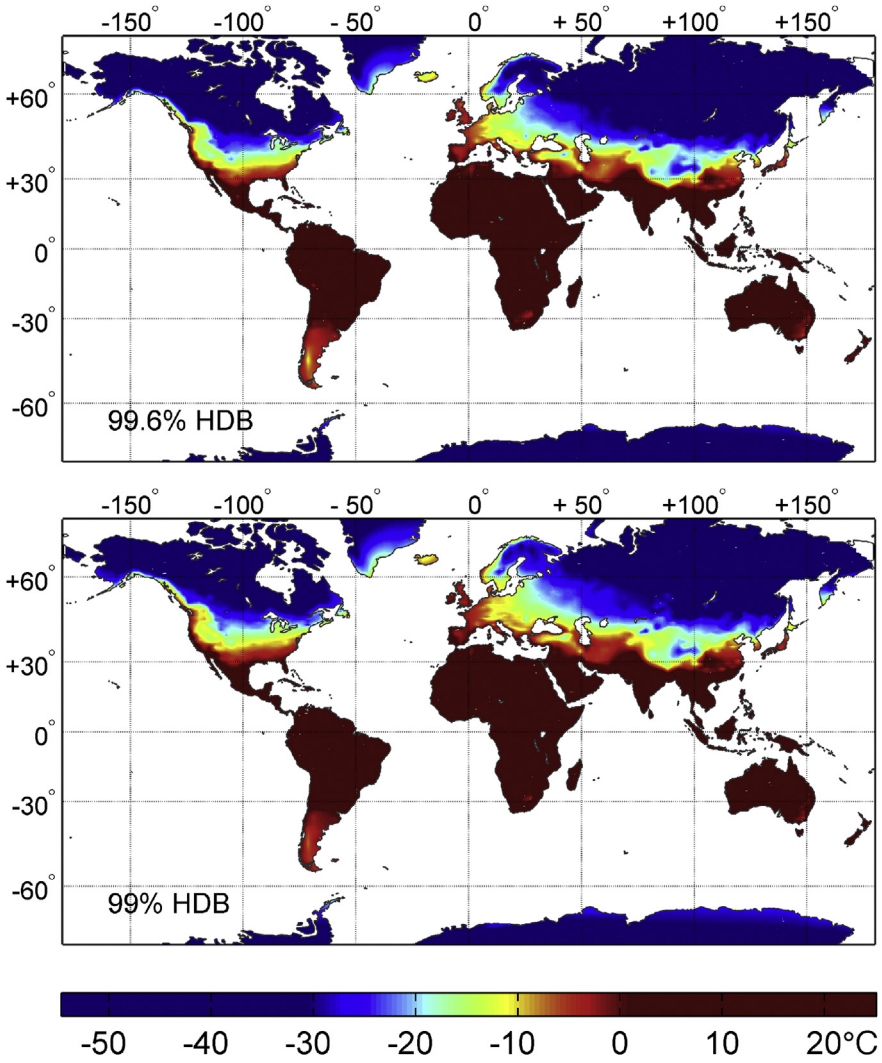

Fig. 6. Distribution of 99.6% and 99% heating dry-bulb (HDB) temperatures.

and *natural neighbor* are investigated for their simplicity and suitability in this research.[5] However, in future, other methods need to be investigated to better account for the effects of altitude.

2.3.1. Triangulation with linear interpolation

In this method, a set of optimal *Delaunay* triangles is created by drawing lines connecting the scattered data points. The point clouds are connected such that no triangle edges are intersected by other triangles. In other words, no point of a triangle is inside the circumference of another triangle [36]. This results in a patchwork of triangulated faces over the grid extent, with each triangle defining a plane over the grid node lying within the triangle. The tilt and elevation of the triangular plane are determined by the three original data points defining the triangle. The attribute value (z_k) can then be found by applying linear interpolation, which can be achieved using matrix determinants. A plane surface through three points $\{x_i,y_i,z_i\}, i = 1,2,3$ in the Euclidian space has a formula in determinant form of [32]:

$$\begin{vmatrix} x & y & z & 1 \\ x_1 & y_1 & z_1 & 1 \\ x_2 & y_2 & z_2 & 1 \\ x_3 & y_3 & z_3 & 1 \end{vmatrix} = 0 \tag{9}$$

The attribute value can now be estimated by evaluating the determinant in the equation. The method uses original data to define the triangles and the resulting surface; therefore, the interpolated data retains the characteristics of source data very closely. Another feature of triangulation is that in areas of densely spaced sampling points, the method can preserve break lines (i.e., discontinuity). However, triangulation with linear interpolation works best in situations where sampling (or measurement) points in the source data are evenly distributed. As an exact interpolation technique, the method does not extrapolate attribute values beyond the range of the data.

2.3.2. Nearest neighbor method

The nearest neighbor method is a simple technique whereby each grid intersection; i.e, attribute value, z_k, is assigned the value

[5] Kriging, an interpolation method, was not investigated in this research as the subjectivity, complexity and subtle variations of the implementation of kriging warrants a detailed investigation of its own. For example, ordinary kriging assumes second-order stationarity and isotropy [33], which did not appear to be the case for the HOF'09 dataset. The other variants such as universal kriging, co-kriging and indicator kriging are based on the assumption that response and explanatory variables have a linear relationship [34], which is not always the case for natural processes [35].

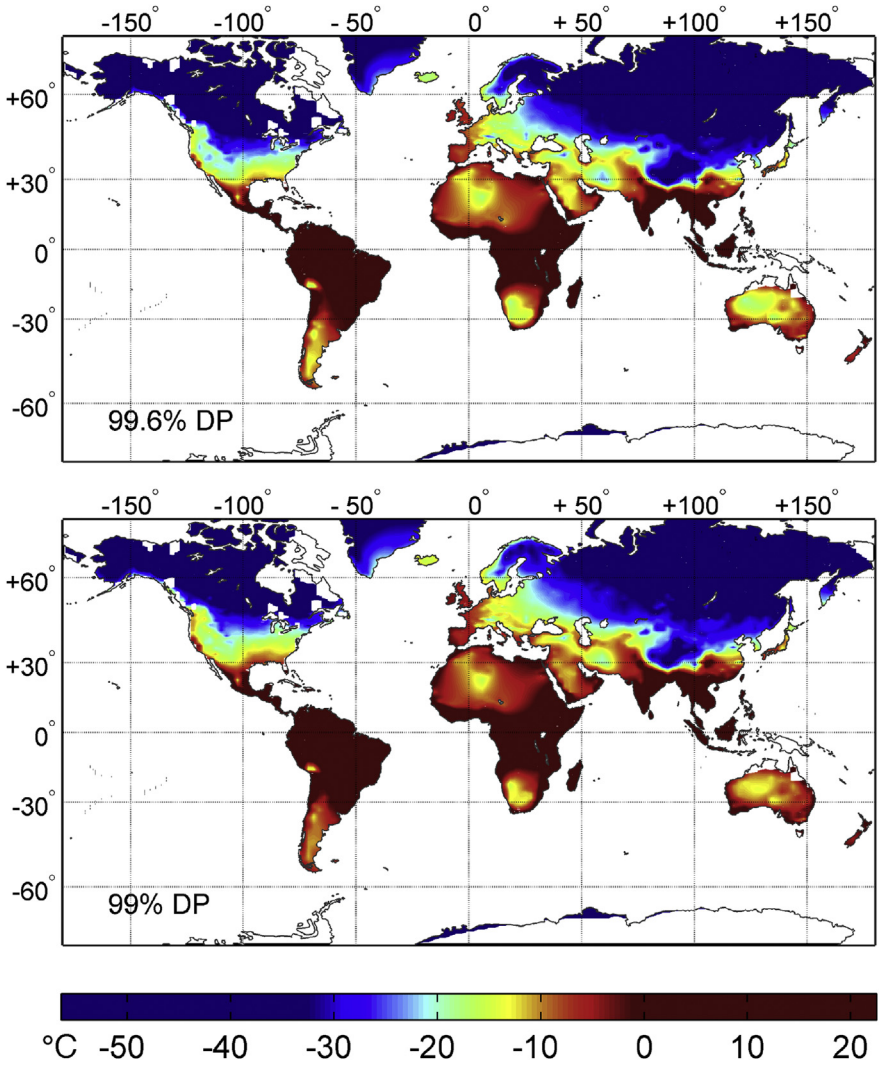

Fig. 7. Distribution 99.6% and 99% dew point (DP) temperatures.

of the nearest point in the input dataset [37]. Such assignments result in a stepped surface, which are not always suitable for interpolating data that are not evenly spaced or in situations where spatial frequency is different for the source and interpolated datasets. Nearest neighbor technique is, however, applicable in situations where there is a need to substitute missing values in a grid where most cells are complete [38]. Other applicable circumstances include situations where steps are expected to be the most appropriate representation of the underlying data and/or where there is concern over the continuity of the underlying field [32].

2.3.3. Natural neighbor method

Natural neighbor interpolation [31] is based on *Voronoi*[6] tessellation, also known as *Dirichlet* or *Thiessen* tessellation. The method creates weights for each of the input points based on their assumed area of influence, which is determined by generating Voronoi polygons around each input point. When a new point (target) is added to the set, the Voronoi diagram changes. Some of the polygons shrink in size, while none increases in size. The area associated with the target's Voronoi polygon occupies parts of the area of its neighboring points' unaffected polygons; i.e., the area of the target's Voronoi polygon is taken from an existing polygon and is called the *borrowed area*. The method uses a weighted average of the neighboring observations, where the weights are proportional to the *borrowed area*. The procedure is explained below with an example, in which data from five neighboring meteorological stations are interpolated to a regularly spaced grid.

Consider five meteorological stations around Birmingham, United Kingdom: Shobdon [WMO[7]: 35200; 52.25° N, 2.88° W], Madley [WMO: 35210, 52.03° N, 2.85° W], Shawbury [WMO: 34140, 52.8° N, 2.67° W], Pershore [WMO: 35290, 52.15° N, 2.03° W] and Birmingham International Airport [WMO: 35340, 52.45° N, 1.73° W]. An attribute (e.g., mean temperature) in these scattered data points need to be interpolated to a regularly spaced point p. The resulting Voronoi diagram with these five stations is given in Fig. 2a, with site boundaries drawn in blue. The target point, p is illustrated in Fig. 2b. The addition of p changes the structure of the diagram. The new Voronoi polygon boundaries for point p are

[6] Voronoi tessellation (the dual structure of Delaunay triangulation) refers to the partitioning of a plane with n points into convex polygons such that each polygon contains exactly one generating point. Every point in a Voronoi polygon is closer to its generating point than to any other.

[7] World Meteorological Organization station identifier.

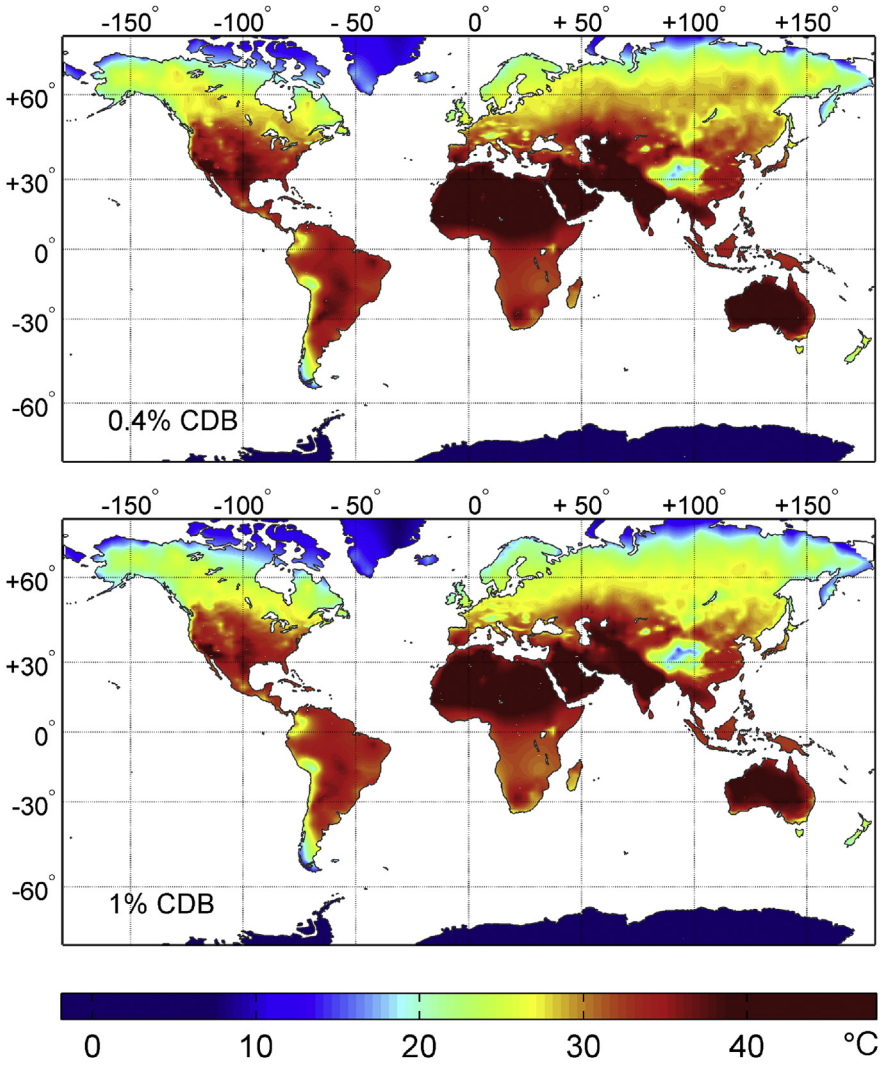

Fig. 8. Distribution of 0.4% and 1% cooling dry-bulb (CDB) temperatures.

shown in red in Fig. 2c.

The weights, λ_i from Equations (7) and (8), corresponding to the area of influence of each data points, can be calculated form:

$$\lambda_i = \frac{Area(V(p) \cap V(s_i))}{Area(V(p))} \tag{10}$$

where s_i are the natural neighbors of point p and $V(s_i)$ their associated regions in the original Voronoi diagram (Fig. 2a). $V(p)$ is the area of the Voronoi polygon associated with point p, shown in red in Fig. 2c.

2.3.4. Effects of interpolation methods

To investigate the effect of selected interpolation methods on contouring, the distribution of annual mean temperature, $\overline{T}$ for Continental United States; i.e., the lower 48 states between Canada and Mexico is mapped, following the methods described earlier. The extent of the map is reduced to 23–50° N and 65–128° W to focus on the area of interest. The region has been selected because of the presence of both sparse and dense distributions of reporting stations. Contours are drawn with a solid line and the areas in between are shaded to enhance the identification of patterns. Contours resulting from the use of three interpolation methods are illustrated in Fig. 3. Fig. 3a–c represents triangulation with linear interpolation, natural neighbor and nearest neighbor, respectively.

As expected, nearest neighbor method results in a stepped surface, with noticeable discontinuity around sparse data points. Examples of which can be seen in the Rocky Mountains, between 41° N 108° W and 46° N 112° W, and around the border regions between California and Nevada, between 30° N 110° W and 40° N 120° W. Similar behavior can also be found in five locations in northern Mexico, between 22° N 100° W and 28° N 110° W). Sudden step changes appear to be associated with sparse data points when compared against the location map of the stations in Fig. 1. In contrast, both linear and natural neighbor methods produce smoother surfaces. Latitudinal variations are more pronounced in both these methods, which agree with conventional wisdom [39]. Natural neighbor method, however, produces a smoother surface than triangulation with linear interpolation method, in which some triangulated artifacts can be seen around the Rocky Mountains. Therefore, natural neighbor has been selected as the method of interpolation in this research.

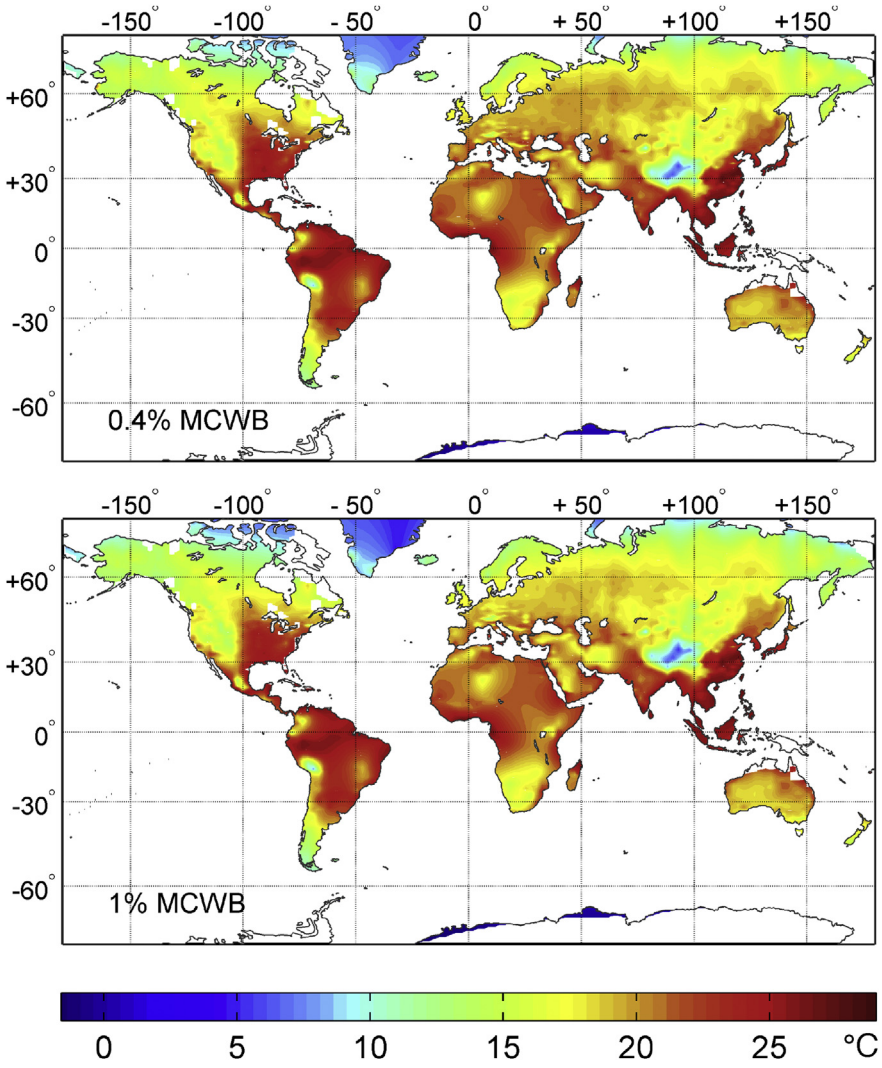

Fig. 9. Distribution of 0.4% and 1% mean coincident wet-bulb (MCWB) temperatures.

3. Results and discussion

3.1. Distribution of mean temperature

3.1.1. Annual mean temperature

Global distribution of annual mean temperature, $\overline{T}$ is illustrated in Fig. 4. $\overline{T}$ varies between −22.6 °C and 31.2 °C.[8] Mean temperature is generally highest in low latitudes and lowest toward the poles. The warmest region lies mostly between 30° N and 30° S latitudes. Areas between 30° N and 60° N have moderate annual mean temperatures. Similar latitudinal areas in the southern hemisphere (30–60° S) have less landmass and therefore, variations in $\overline{T}$ are less pronounced.

Regions of high temperature can be found in Saharan Africa, some parts of Asia and in South America. Regions with high $\overline{T}$ in Asia are typically characterized by warm-humid (15° N-15° S) and composite monsoon climates. In contrast, high $\overline{T}$ regions in Africa (in particular Saharan Africa) are characterized by arid climate. Each of these regions presents particular challenge for environmental design of buildings due to the varying moisture content in the air and its diurnal and seasonal distributions. High temperatures over Saharan Africa are considered to be due to clear skies and small solar zenith angles combined with negligible evapotranspiration [40]. Anomalies in the longitudinal distribution of $\overline{T}$ have associations with topography and distance from the nearest coastline. $\overline{T}$ is lower in mountainous regions, compared to the neighboring areas of same latitude. The effect of elevation is visible in the Himalayas in Southeast Asia, Andes in South America, Rockies in the United States and Alps in Europe. These effects are more pronounced with finely spaced isolines in regions where meteorological stations are closely spaced. Polar region in the south is cooler than its northern counterpart, which has been suggested as an effect of elevation by Legates et al. [40].

3.1.2. Monthly mean temperature

Twelve contour maps of monthly mean temperature, $\overline{T}_m$, are given in Fig. 5. The lowest monthly mean temperature in the dataset is −41.9 °C in Curapca, Russia [WMO: 247680] in January, while the highest monthly mean temperature is 38.3 °C in Kuwait International Airport, Kuwait [WMO: 405820] in July. The minimum monthly mean temperature ranges from −41.9 °C to −23.7 °C,

[8] The extremes of $\overline{T}$; i.e., the minimum and maximum $\overline{T}$ may be different if all locations on earth were included in the HOF'09 dataset. Therefore, the range of $\overline{T}$ needs to be interpreted within the context of data coverage in the HOF'09 dataset.

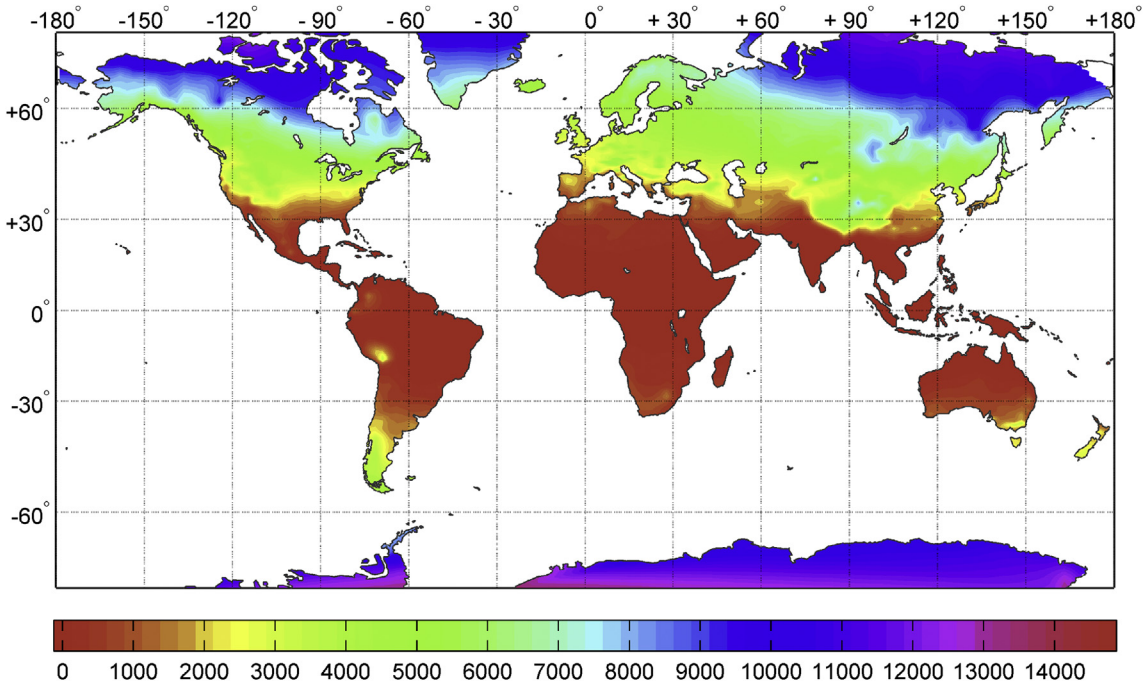

Fig. 10. Distribution of annual heating degree-days at 18.3° C, $HDD_{18.3}$ (° C-day).

while the maximum ranges from 31.8 °C to 38.3 °C. In line with the distribution of annual mean temperature, the monthly distributions show the effects of latitude and elevation. The effect of mountain ranges such as the Rockies, Andes, Alps and Himalayas is more pronounced in summer months. The effect of the Himalayas is more pronounced than other mountain ranges due to its area and elevation. The seasonal swing in mean temperature is more pronounced in high latitude areas and less pronounced in the low latitude (15° N-15° S) and warmer areas in Africa, Australia and in some parts of Asia and South America.

July is the warmest month in the northern hemisphere, with significant temperatures in mid latitudes in North America, Europe and Asia. Seasonal variations also highlight another important aspect of environmental design of buildings. At present, the seasonal distribution of mean temperature in cold and temperate climates is such that it does not require comfort cooling or air-conditioning in majority of the buildings, in particular in domestic buildings. In other words, system design only concerns with the design for heating season and does not require additional capital and maintenance cost for cooling systems. This may change in future when the projections of increased surface temperatures are realized. Even a conservative estimate of 1.8 °C by 2100 [9] may tip the balance for a number of locations in Europe, North America and colder regions of Asia. Both heating and cooling systems may need to be designed and maintained for majority of the buildings in future, the initial evidence of which is already being seen in the increased installations of air-conditioning systems in the UK and Europe [41]. Another challenging aspect of increased temperature may be that the transitional periods between heating and cooling seasons may increase in temperate climates such as Denmark[9] [43]. Transitional periods are the time of year when heating and cooling systems may need to operate on the same day.

[9] Denmark's climate is more specifically classed as CfB – warm temperate humid with warm summer [42].

3.2. Design temperatures for peak operations

Information on dry-bulb, wet-bulb and dew-point temperatures at various frequencies of occurrence are used for the design of heating and cooling systems considering various operational peak conditions. Design temperatures in the HOF′09 dataset are reported on annual percentile basis. For warm-season, temperature and humidity conditions are reported on annual percentiles of 0.4, 1.0 and 2.0; i.e., 0.4%, 1.0% and 2.0% annual occurrences. In contrast, cold-season conditions are based on annual percentiles of 99.6 and 99.0; i.e., 99.6% and 99% annual occurrences. The percentiles refer to the percentages of year the reported temperature is greater. For example, $HDB_{99.6}$ means that for 99.6% of the time (= 8725hr) of year, dry-bulb temperatures are above the reported $HDB_{99.6}$ where as $CDB_{0.4}$ means that for 0.4% of the time (= 350hr) of year, dry-bulb temperatures are above the reported $CDB_{0.4}$. The use of percentile information depends on the nature of application. For example, 1% cooling dry bulb (CDB) and 99% heating dry bulb (HDB) are used for system sizing in general applications such as domestic and non-domestic buildings while 0.4% CDB and 0.4% HDB are typically used for mission critical applications [44] such as operating theaters in hospitals. Peak design condition information such as *HDB* and *CDB* enables the sizing of heating, cooling, humidification, dehumidification and ventilation systems.

Fig. 6 illustrates the distribution of 99.6% and 99% heating dry-bulb (HDB) temperatures, used in the design of services systems for cold season operation. Fig. 7 shows the distribution of 99.6% and 99% dew point (DP) temperatures. Distributions of $HDB_{99.6}$ and $DP_{99.6}$ are similar in pattern. However, some differences between heating dry-bulb and dew-point temperatures can be seen in arid regions; e.g., northern Africa (*Sahara*) and northwest part of Indian sub-continent (*Thar*). These locations are also characterized by high daytime temperature and low nighttime temperature. Changes in the distribution of $HDB_{99.6}$ and $DP_{99.6}$ in these regions, therefore, may be of relevance in understanding the impact of climate change, as well as the strategies for adaptation.

Fig. 8 and Figure Fig. 9 shows the distribution of 0.4% and 1%

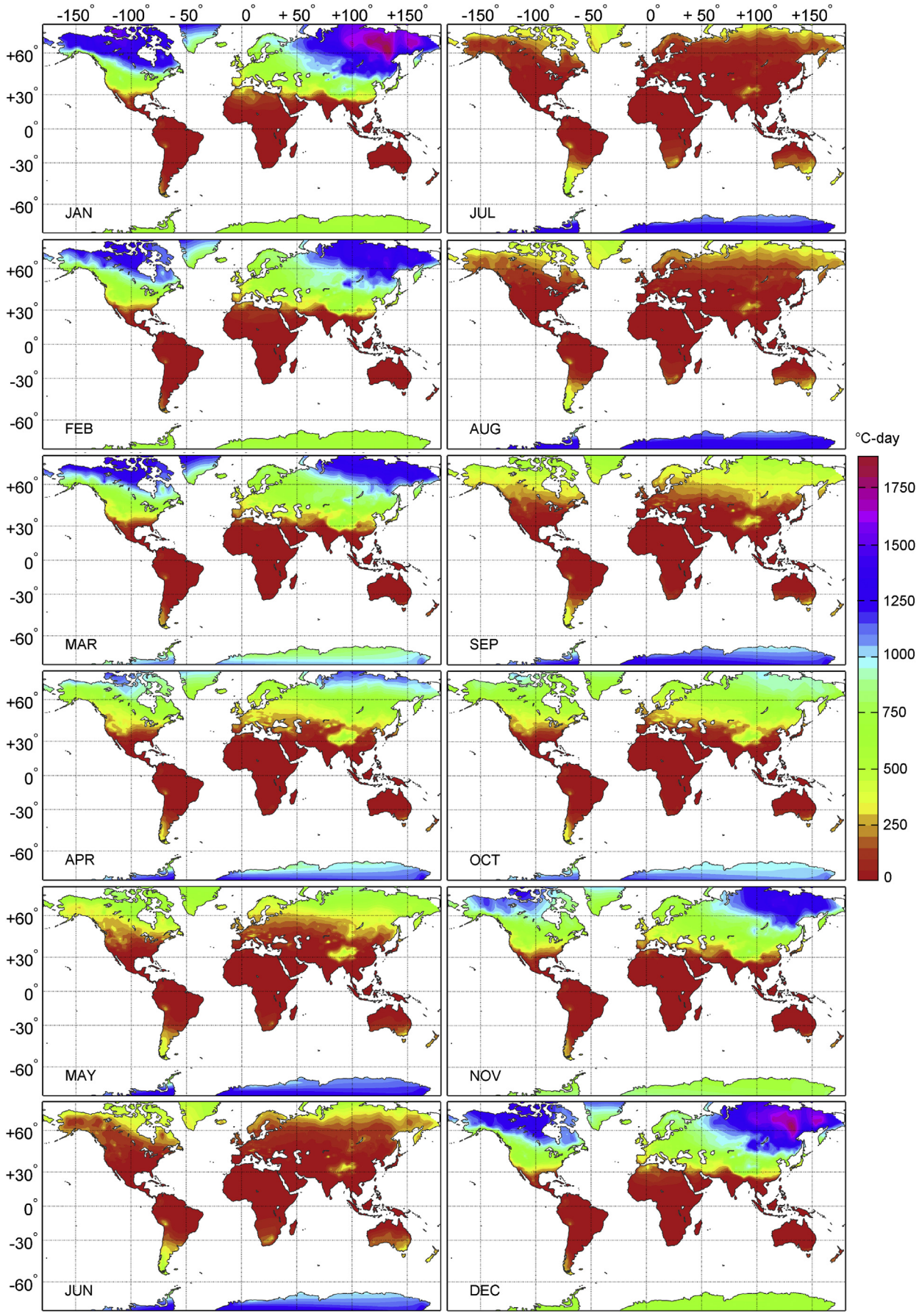

Fig. 11. Distributions of monthly heating degree-days at 18.3° C, $MHDD_{18.3}$ (° C-day).

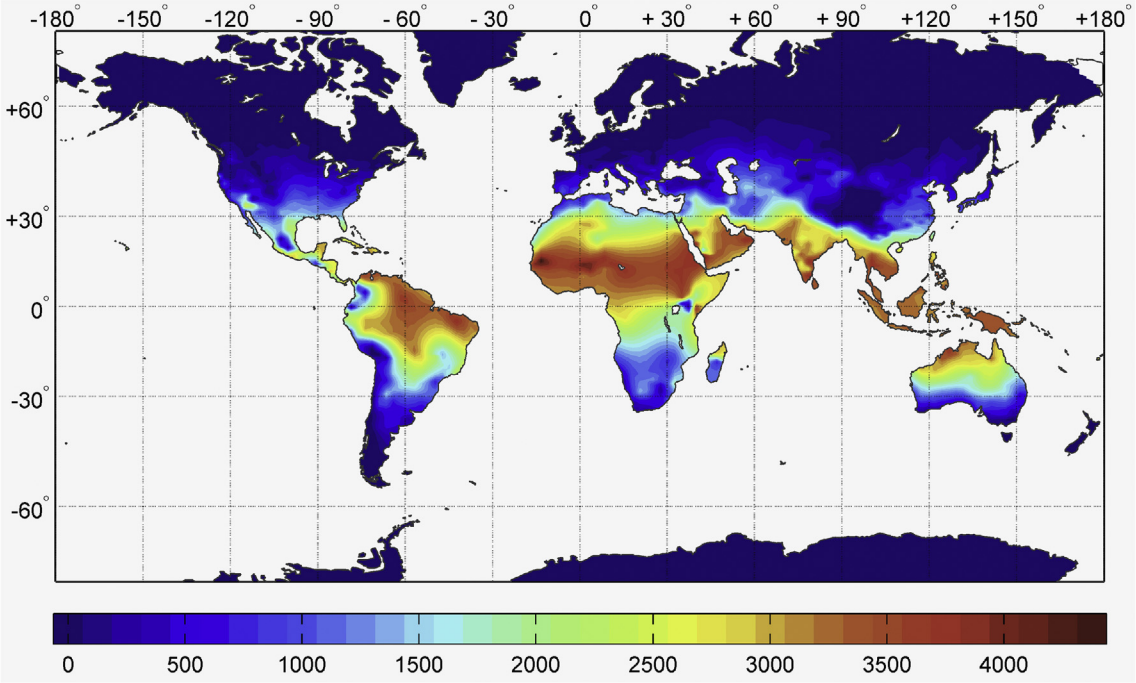

Fig. 12. Distribution of annual cooling degree-days at 18.3° C, $CDD_{18.3}$ (° C-day).

cooling dry-bulb (CDB) and mean coincident wet-bulb (MCWB) temperatures respectively. The distribution of 0.4% cooling dry-bulb temperature illustrate that $CDB_{0.4}$ is high 10s to low 20s in high latitudes (¿60° N), high 20s to low 30s in mid latitudes (30–60° N) and high 30s to low 40s in low latitudes (0–30° N). Higher $CDB_{0.4}$ (in mid 40s) can be found in Australia, the Middle-East, northern Africa and the Indian Sub-continent, characterized by arid climate. Although latitudinal variances are pronounced in the $CDD_{0.4}$ distribution map, there are significant areas with similar, if not same, cooling dry-bulb temperatures. The pattern of distribution is also similar for $MCWB_{0.4}$, albeit, as expected, the magnitude is smaller.

3.2.1. Heating degree-days

Annual heating degree-days at base temperature 18.3 °C, $HDD_{18.3}$, is illustrated in Fig. 10. The minimum $HDD_{18.3}$ is 0° C-day. The maximum $HDD_{18.3}$, 14958° C-day, in the ASHRAE–HOF database is for Siple Dome, Antarctica [WMO ID: 893450], which incidentally has the lowest $\overline{T}$ in the dataset. The distribution follows overall trends in annual mean temperature, $\overline{T}$. In line with the distribution of $\overline{T}$, the warmest region lies mostly between 30° S and 30° N latitudes; i.e., heating degree-days are lower – mostly around zero, in this region. Although the maximum $HDD_{18.3}$ in this region (30° S–30° N) is 6357° C-day, the median is only 37° C-day. $HDD_{18.3}$ for almost all of Africa, and significant parts of South America, northern Australia and Asia (mostly southeastern part) is zero. The effect of latitude in the remaining regions is evident in the distribution map. However, the effect of elevation is somewhat less pronounced for $HDD_{18.3}$ than $\overline{T}$. One of the reasons may be the effect of seasonal or monthly variations in the distribution of mean temperature, which may result in a reduction in the magnitude of variance in annual degree-days.

Twelve distribution maps of monthly heating degree-days at 18.3 °C, $MHDD_{18.3}$ are given in Fig. 11. Some interesting patterns can be seen in the distribution maps. Higher $MHDD_{18.3}$ s are concentrated in high latitude areas in the northern hemisphere, particularly in Siberia. $MHDD_{18.3}$ is higher in the northern hemisphere during December and January; i.e., the cold season. Opposite scenario can be found in the southern hemisphere, as the seasons in the northern and southern hemispheres are six months out of phase. $MHDD_{18.3}$ s toward the South Pole are lower when it is cold season in the northern hemisphere and warm season in the southern hemisphere. Southern Australia is colder than the northern Australia due to the distance from the Equator. The effect of high elevation can also be seen in monthly distributions of heating degree-days; e.g., regions around the Himalayas.

3.2.2. Cooling degree-days

Annual cooling degree-days at base temperature 18.3 °C, $CDD_{18.3}$, is illustrated in Fig. 12. The minimum $CDD_{18.3}$ is 0° C-day, while the maximum is 4701° C-day in the ASHRAE–HOF database. In line with the distribution of annual mean temperature and $HDD_{18.3}$, the warmest region (i.e., with higher $CDD_{18.3}$) lies between 30° S and 30° N latitudes. The mean, median and standard deviation of $CDD_{18.3}$ in this region (30° S–30° N) are 2338, 2391 and 1034° C-day, respectively. The effect of elevation, as well as that of latitude, is pronounced in this distribution map. The effects can be seen in all continents where $CDD_{18.3}$ is greater than zero. The regions of higher $CDD_{18.3}$ are located in low latitudes of South America, Saharan Africa, the Middle East and Southeast Asia. Makkah, Saudi Arabia [WMO ID: 410300] has the highest $CDD_{18.3}$.

Twelve distribution maps of monthly cooling degree-days at 18.3 °C, $MCDD_{18.3}$ are given in Fig. 13. The seasonal distributions suggest that $MCDD_{18.3}$ is lower during cold season and higher during warm season. Regions with higher monthly cooling degree-days appear to be concentrated between 0 and 30° N latitudes, in particular in Africa and the Middle East. Some regions in South America, Africa, southern Asia (including the tropical belt) and northern Australia have higher than zero $MCDD_{18.3}$ all year round, indicating the cooling dominated nature of their climate.

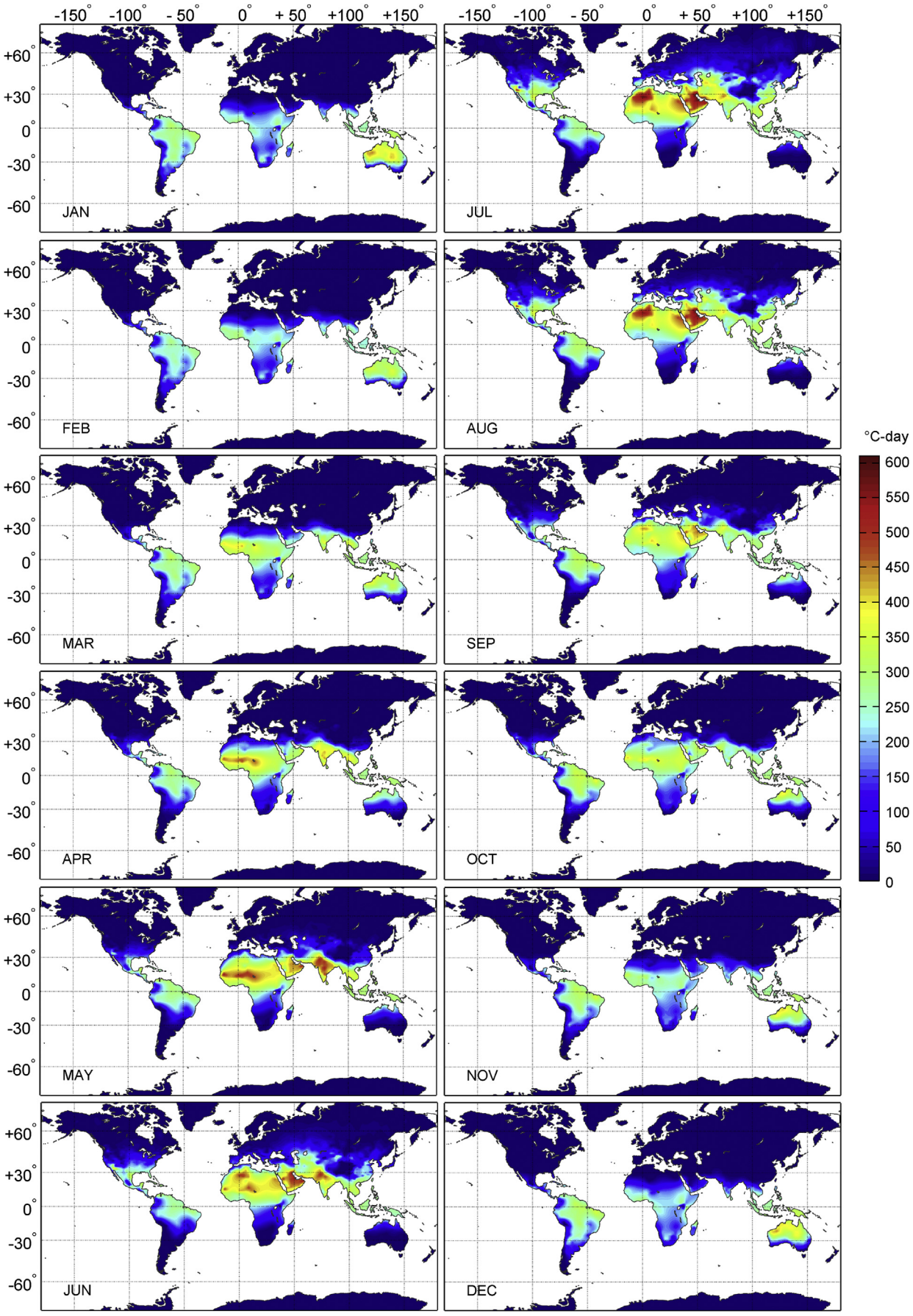

Fig. 13. Distributions of monthly cooling degree-days at 18.3° C, $MCDD_{18.3}$ (° C-day).

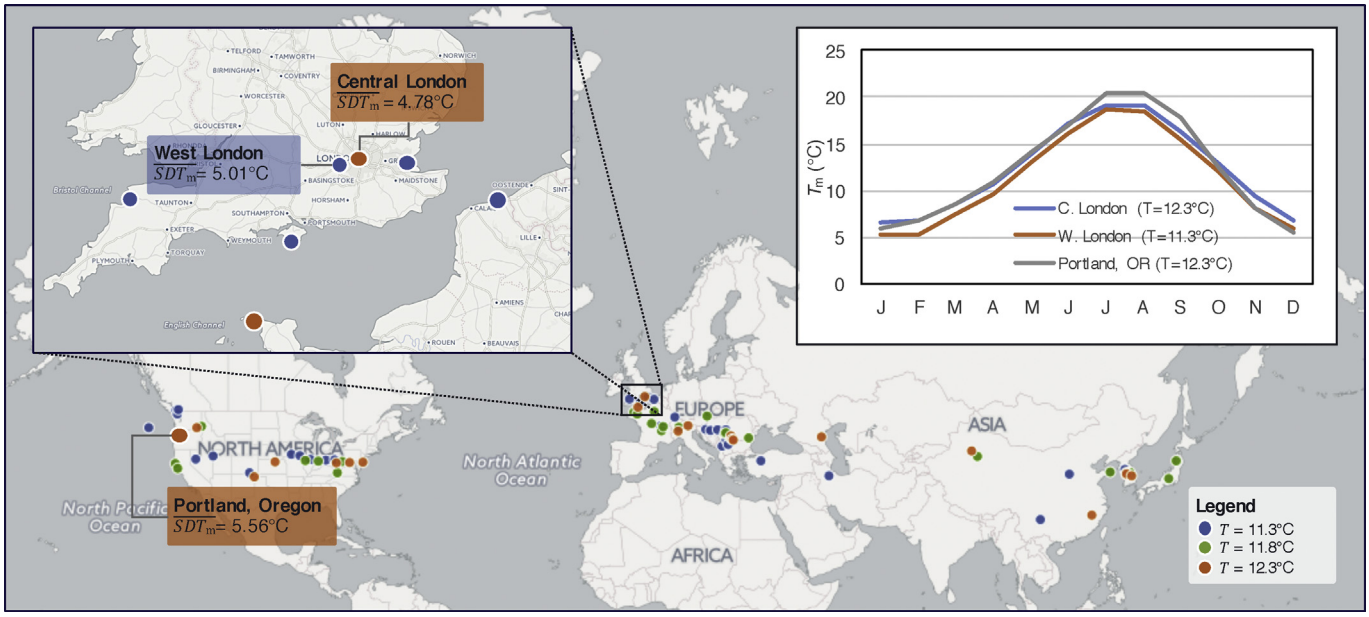

Fig. 14. The identification of analogous climates.

4. Remarks

4.1. Data resolution

Investigation into the global distribution of climatic design conditions depends, to a large extent, on the geospatial distribution of the reporting stations. Although, the reporting stations in the HOF′09 dataset are widely distributed and the resolution of the data is higher than previous releases [5], there is a need for higher resolution in some regions. Most of Africa, South America and parts of Asia need to be represented better, especially in the regions of interest. For example, Saharan and Sub-Saharan regions have geographical features, which may result in subtle variations and could be captured better with a higher resolution dataset of the region. Stations in Antarctica and Greenland are mostly located in the coastal belt. More inland stations could be incorporated in future releases. Of note, these are sparsely populated and therefore the interest in climatic design conditions of these regions may be low. There is an effect of elevation, which is responsible for some longitudinal anomalies, as discussed in previous sections. Therefore, stations around high elevation areas need to be better represented. For example, the number of stations around the Andes, covering western part of South America (Argentina, Bolivia, Chile, Columbia, Ecuador, Peru and Venezuela), could be increased.

4.2. Climate change

Projected increases in temperature due to anthropogenic climate change make it necessary to integrate the understanding of geospatial distributions of climatic design information in the education and practice of building design professionals. The consideration of climate in building design has always been static; i.e., the climate of the site remains fixed for the lifespan of a building, typically 40–50 years. Designers and facility managers are now faced with a changing climate and the rate of change is faster than ever. They need to consider projected future climates (e.g., every 20 years), in addition to the present-day based on past observed data, to ensure that buildings are resilient and future-proof. The consideration of multiple climates in a single design problem will require advanced visualization at various spatial and temporal scales, if uncertainties of climate projections are to be reconciled.

There is potential for the use climate database for the identification of climate analogs; i.e., climates that are similar in nature. The *future climate analog* – a present-day climate that is similar in nature to the projected future climate of a location, can offer insights into the energy and environmental performance of a building for a given design or strategy that is based on an understanding of the present-day context. The development of a detailed methodology for identifying analogous climate is outside the scope of the paper. However, Fig. 14 illustrates the concept of the identification of future climate analogs using the West London weather station (WMO: 37720), located in London Heathrow Airport. Present day annual mean temperature, $\overline{T}$ of West London is 11.3 °C. Climates with the same $\overline{T}$ has the potential to be present-day climate analogs to West London and are depicted as blue dots in the figure. Southern hemisphere locations are omitted for brevity. Matching only the annual mean temperature, $\overline{T}$, may not result in a climate of similar distribution. Previous studies [24,30] have found the standard deviation of mean temperature to be an important indicator for the severity and duration of hot and cold weather; i.e., degree-days. As a first step, one would be inclined to match mean standard deviations of monthly average temperature, $\overline{SDT}_m$ as a proxy for the distribution over a year.

Let us consider the scenario of 1 °C rise in annual mean temperature, for which we would like to find future climate analog to West London's present-day climate. Present-day climates with $\overline{T} = 11.3 + 1 = 12.3^\circ$ C are selected from the ASHRAE–HOF database and are represented as orange dots in Fig. 14[10]. There are 20 worldwide locations with $\overline{T} = 12.3$ °C but of varying $\overline{SDT}_m$, ranging from 3.84 to 11.87. Locations in the southern hemisphere are omitted in the figure for brevity. Climates with higher standard deviations have colder winter and warmer summer than West London. Two locations – Central London (WMO: 37790, $\overline{SDT}_m = 5.01$) in the UK and Portland, Oregon (WMO: 726959, $\overline{SDT}_m = 5.56$)

[10] Climates with $\overline{T} = 11.8^\circ$ C, corresponding to a 0.5° C rise in temperature are shown as green dots for contextualisation only.

in the USA have closest $\overline{SDT}_m$ to West London's 4.78. Mean monthly temperatures, $\overline{T}_m$ of three locations are shown in the inset. The distributions demonstrate similar patterns of winter and summer; the curve for Portland, however, showing higher $\overline{T}_m$ in the summer. Both future climate analogs, Central London and Portland, Oregon appear plausible and within the range of uncertainties presented in previous studies on UK climate projections [45].

4.3. Future work

There is significant potential for the extraction and use of knowledge on climate parameters in enhancing the design and operation of buildings, energy infrastructure and associated systems [3]. Research reported here can be considered as a starting point for further work, some of which are listed below:

- One obvious direction is the analysis of the spatial impacts of climate change on the design of buildings and cities, in particular the effects of urban heat island. As seen in the previous section, within the 20 km city of London, the difference in annual mean temperature is 1 °C, which is quite significant. Impact and adaptation studies will, therefore, need to look into high resolution spatial variabilities, especially for large agglomerations.
- Knowledge of climatic variability can be used as inputs or boundary conditions in downstream applications such as design sensitivity analysis. An example of such analysis is the investigation into the effects of the choice envelope construction materials on energy and environmental performance of buildings [46].
- Another direction is the identification and development of suitable sites for large-scale energy systems that depend on climatic variabilities.
- Improved visualization techniques can enable the superimposition of multiple parameters of interest in one single map or multi-dimensional visualization artifacts [47] for enhanced knowledge extraction. For example, population projection can be visualized along with temperature distribution to identify potential risks for human-centric systems.
- Policy development is another area that can benefit from an improved understanding of geospatial distributions. Energy simulation and modeling for compliance, especially degree-day based [48] will benefit from spatial localizations.
- While there are numerous studies on spatial distributions of climate normals such as annual and monthly temperatures, there is a gap in literature on the normals used by the building industry; e.g. heating and cooling degree-days, and percentiles. Further work can be carried out on interpolation techniques, suited to the dataset.
- This research presented the concept of the identification of climate analogs, which needs further work on the development and validation of the method.

5. Conclusion

The understanding of climatic design conditions is an essential first step for effective design and operation of energy efficient buildings. This paper explored geospatial distributions of temperature, a key climatic design information of a site, and relevant parameters that were derived from the temporal distribution of temperature. Together, the investigated parameters are typically used as boundary design conditions for many applications, from the design of building form and layout to the design and operation of heating, cooling, ventilation, humidification and dehumidification systems. Latitudinal variations are prominent in most of the distribution maps. Longitudinal anomalies are present, which appear to have links with topography, vegetation and elevation. Variations in heating and cooling degree-days appear to have a considerable relationship with annual mean temperature, as their distributions appear similar.

The use of temperature and related climatic design information in every step of the process of environmental design of buildings suggest that the understanding of their geospatial distribution is essential. Projected changes in climate and the need to learn from successful and failed design strategies in analogous (present–day and future) climates will increase the importance of the geospatial understanding of climate in the design process. Constructed distribution maps are envisaged to serve as baseline maps of the present-day climate, which can be used for comparison with future climates. The methodology described in this paper can also be used for detailed investigations into present-day and future regional climates and their characteristics.

Acknowledgment

The author acknowledges the financial support of the European Commission under the 7th Framework Programme (FP7). Grant reference: 619682.

References

[1] S. Austin, A. Newton, J. Steele, P. Waskett, Modelling and managing project complexity, Int. J. Proj. Manag. 20 (3) (2002) 191–198.
[2] S. Macmillan, J. Steele, S. Austin, P. Kirby, R. Spence, Development and verification of a generic framework for conceptual design, Des. Stud. 22 (2) (2001) 169–191.
[3] M. Mourshed, Interoperability-based Optimisation of Architectural Design, PhD thesis, National University of Ireland, Cork, Ireland, Cork, Ireland, 2006.
[4] M. Mourshed, D. Kelliher, M. Keane, Green architecture: the need for climate analysis and thermal simulation during early stages of design, Glob. Built Environ. Rev. 5 (2) (2005) 12–20.
[5] ASHRAE, ASHRAE Handbook: Fundamentals, American Society of Heating, Refrigerating and Air-Conditioning Engineers, Atlanta, GA, 2009.
[6] O. Akin, Case-based instruction strategies in architecture, Des. Stud. 23 (4) (2002) 407–431.
[7] B.H. Eilouti, Design knowledge recycling using precedent-based analysis and synthesis models, Des. Stud. 30 (4) (2009) 340–368.
[8] J.W. Robinson, Design as exploration, Des. Stud. 7 (2) (1986) 67–79.
[9] IPCC, Summary for policymakers, in: Climate Change 2007: Synthesis Report: Fourth Assessment Report of the Intergovernmental Panel on Climate Change, Cambridge University Press, New York, NY, 2007, pp. 1–22.
[10] C.H. Sanders, M. Phillipson, UK adaptation strategy and technical measures: the impacts of climate change on buildings, Build. Res. Inf. 31 (3–4) (2003) 210–221.
[11] S. Shikder, M. Mourshed, A.D. Price, Summertime impact of climate change on multi-occupancy British dwellings, Open House Int. 37 (4) (2012) 50–60.
[12] S.E. Belcher, J.N. Hacker, D.S. Powell, Constructing design weather data for future climates, Build. Serv. Eng. Res. Technol. 26 (1) (2005) 49–61.
[13] P.H. Shaikh, N.B.M. Nor, P. Nallagownden, I. Elamvazuthi, T. Ibrahim, A review on optimized control systems for building energy and comfort management of smart sustainable buildings, Renew. Sustain. Energy Rev. 34 (2014) 409–429.
[14] EC, Energy Performance of Buildings Directive (Recast) 2010/31/EU, European Commission, Brussels, BE, 2010.
[15] IRENA, Global Atlas for Renewable Energy, 2016. http://irena.masdar.ac.ae/.
[16] Meteotest, Meteonorm – a Comprehensive Meteorological Reference, 2016. http://meteonorm.com.
[17] UK Meteorological Office, MIDAS Land Surface Stations Data, 2012. http://badc.nerc.ac.uk/.
[18] K. Skeiker, Comparison of methodologies for TMY generation using 10 years data for Damascus, Syria, Energy Convers. Manag. 48 (7) (2007) 2090–2102.
[19] ASHRAE, American society of heating refrigeration and Air-Conditioning engineers, http://www.ashrae.org/(2012).
[20] CIBSE, Chartered institution of building services engineers, http://www.cibse.org/(2012).
[21] SWERA, Data for Solar and Wind Renewable Energy, 2016. http://en.openei.org/wiki/SWERA/Data.
[22] D. Thevenard, R. Humphries, The calculation of climatic design conditions in the 2005 ASHRAE Handbook – Fundamentals, ASHRAE Trans. 111 (1) (2005) 457–466.
[23] D. Thevenard, Updating the ASHRAE Climatic Data for Design and Standards (RP-1453), American Society of Heating Refrigeration and Air-Conditioning

Engineers, Atlanta, GA, 2009.
[24] M. Mourshed, Relationship between annual mean temperature and degree-days, Energy Build. 54 (2012) 418–425, http://dx.doi.org/10.1016/j.enbuild.2012.07.024.
[25] L. Yang, J.C. Lam, C.L. Tsang, Energy performance of building envelopes in different climate zones in China, Appl. Energy 85 (9) (2008) 800–817.
[26] J. Yu, C. Yang, L. Tian, D. Liao, A study on optimum insulation thicknesses of external walls in hot summer and cold winter zone of China, Appl. Energy 86 (11) (2009) 2520–2529.
[27] R. Fayaz, B.M. Kari, Comparison of energy conservation building codes of Iran, Turkey, Germany, China, ISO 9164 and EN 832, Appl. Energy 86 (10) (2009) 1949–1955.
[28] M. Mourshed, The impact of the projected changes in temperature on heating and cooling requirements in buildings in Dhaka, Bangladesh, Appl. Energy 88 (11) (2011) 3737–3746.
[29] ASHRAE, Energy Standard for Buildings except Low-rise Residential Buildings, American Society of Heating Refrigeration and Air-Conditioning Engineers, Atlanta, GA, 2010.
[30] G.J. Schoenau, R.A. Kehrig, Method for calculating degree-days to any base temperature, Energy Build. 14 (4) (1990) 299–302.
[31] R. Sibson, A brief description of natural neighbor interpolation, in: V. Barnett (Ed.), Interpreting Multivariate Data, John Wiley, Chichester, UK, 1981, pp. 21–36.
[32] M.J. de Smith, M.F. Goodchild, P.A. Longley, Geospatial Analysis: a Comprehensive Guide to Principles, Techniques and Software Tools, Matador, Leicester, UK, 2007.
[33] I.A. Nalder, R.W. Wein, Spatial interpolation of climatic normals: test of a new method in the Canadian boreal forest, Agric. For. Meteorology 92 (4) (1998) 211–225.
[34] J. Aalto, P. Pirinen, J. Heikkinen, A. Venäläinen, Spatial interpolation of monthly climate data for Finland: comparing the performance of kriging and generalized additive models, Theor. Appl. Climatol. 112 (1) (2012) 99–111.
[35] J. Hjort, M. Luoto, Novel theoretical insights into geomorphic processâĂŞenvironment relationships using simulated response curves, Earth Surf. Process. Landf. 36 (3) (2011) 363–371, http://dx.doi.org/10.1002/esp.2048.
[36] M. de Berg, C. Otfried, M. van Kreveld, M. Overmars, Computational Geometry: Algorithms and Applications, Springer-Verlag, Berlin, Germany, 2008.
[37] G.J. Grevera, J.K. Udupa, An objective comparison of 3-D image interpolation methods, IEEE Trans. Med. Imaging 17 (4) (1998) 642–652.
[38] H.M. Yilmaz, The effect of interpolation methods in surface definition: an experimental study, Earth Surf. Process. Landf. 32 (9) (2007) 1346–1361.
[39] C.D. Ahrens, Meteorology Today: an Introduction to Weather, Climate, and the Environment, Thomson Brooks/Cole, Belmont, CA, 2007.
[40] D.R. Legates, C.J. Willmott, Mean seasonal and spatial variability in global surface air temperature, Theor. Appl. Climatol. 41 (1–2) (1990) 11–21.
[41] BSRIA, European Market for Air Conditioning, Building Services Research and Information Association, Bracknell, UK, 2008.
[42] M. Kottek, J. Grieser, C. Beck, B. Rudolf, F. Rubel, World map of the Köppen-Geiger climate classification updated, Meteorol. Z. 15 (3) (2006) 259–263.
[43] S. Petersen, S. Svendsen, Method for simulating predictive control of building systems operation in the early stages of building design, Appl. Energy 88 (12) (2011) 4597–4606.
[44] USACE, Design: Engineering Weather Data, US Army Corps of Engineers, Washington, DC, 2003.
[45] J. Murphy, D. Sexton, G. Jenkins, P. Boorman, B. Booth, C. Brown, R. Clark, M. Collins, G. Harris, E. Kendon, R. Betts, S. Brown, T.P. Howard, K.A. Humphrey, M. McCarthy, R. McDonald, A. Stephens, C. Wallace, R. Warren, R. Wilby, R.A. Wood, UK Climate Projections Science Report: Climate Change Projections, Met Office Hadley Centre, Exeter, UK, 2009.
[46] R.M. Dowd, M. Mourshed, Low carbon buildings: sensitivity of thermal properties of opaque envelope construction and glazing, Energy Procedia 75 (2015) 1284–1289. http://dx.doi.org/10.1016/j.egypro.2015.07.189.
[47] M. Mourshed, S. Shikder, A.D. Price, Phi-array: a novel method for fitness visualization and decision making in evolutionary design optimization, Adv. Eng. Inf. 25 (4) (2011) 676–687, http://dx.doi.org/10.1016/j.aei.2011.07.005.
[48] S.H. Hong, T. Oreszczyn, I. Ridley, The impact of energy efficient refurbishment on the space heating fuel consumption in english dwellings, Energy Build. 38 (10) (2006) 1171–1181, http://dx.doi.org/10.1016/j.enbuild.2006.01.007.